Defining the Role of Mitochondrial Fission in Corneal Myofibroblast Differentiation

Kye-Im Jeon,[1,3] Ankita Kumar,[1] Kaitlin T. Wozniak,[1,3] Keith Nehrke,[2] and Krystel R. Huxlin[1,3]

[1]Department of Ophthalmology, University of Rochester, Rochester, New York, United States
[2]Department of Medicine - Nephrology Division, University of Rochester, Rochester, New York, United States
[3]Center for Visual Science, University of Rochester, Rochester, New York, United States

Correspondence: Krystel R. Huxlin, University of Rochester Medical Center, Department of Ophthalmology, 601 Elmwood Ave Box 314, Rochester, NY 14642, USA; khuxlin@ur.rochester.edu.

Received: July 30, 2021
Accepted: March 14, 2022
Published: April 4, 2022

Citation: Jeon KI, Kumar A, Wozniak KT, Nehrke K, Huxlin KR. Defining the role of mitochondrial fission in corneal myofibroblast differentiation. *Invest Ophthalmol Vis Sci.* 2022;63(4):2. https://doi.org/10.1167/iovs.63.4.2

Purpose. Fibrosis caused by corneal wounding can lead to scar formation, impairing vision. Although preventing fibroblast-to-myofibroblast differentiation has therapeutic potential, effective mechanisms for doing so remain elusive. Recent work shows that mitochondria contribute to differentiation in several tissues. Here, we tested the hypothesis that mitochondrial dynamics, and specifically fission, are key for transforming growth factor (TGF)-β1–induced corneal myofibroblast differentiation.

Methods. Mitochondrial fission was inhibited pharmacologically in cultured primary cat corneal fibroblasts. We measured its impact on molecular markers of myofibroblast differentiation and assessed changes in mitochondrial morphology through fluorescence imaging. The phosphorylation status of established regulatory proteins, both of myofibroblast differentiation and mitochondrial fission, was assessed by Western analysis.

Results. Pharmacological inhibition of mitochondrial fission suppressed TGF-β1-induced increases in alpha-smooth muscle actin, collagen 1, and fibronectin expression, and prevented phosphorylation of c-Jun N-terminal kinase (JNK), but not small mothers against decapentaplegic 3, p38 mitogen-activated protein kinase (p38), extracellular signal-regulated kinase 1 (ERK1), or protein kinase B (AKT). TGF-β1 increased phosphorylation of dynamin-related protein 1 (DRP1), a mitochondrial fission regulator, and caused fragmentation of the mitochondrial network. Although inhibition of JNK, ERK1, or AKT prevented phosphorylation of DRP1, none sufficed to independently suppress TGF-β1–induced fragmentation.

Conclusions. Mitochondrial dynamics play a key role in early corneal fibrogenesis, acting together with profibrotic signaling. This is consistent with mitochondria's role as signaling hubs that coordinate metabolic decision-making. This suggests a feed-forward cascade through which mitochondria, at least in part through fission, reinforce noncanonical TGF-β1 signaling to attain corneal myofibroblast differentiation.

Keywords: cornea, myofibroblast, TGF-β1, differentiation, mitochondria, fission

Corneal fibrosis can result from traumatic injury, chemical burns, infection, and even surgery.[1] Transparent corneal keratocytes differentiate into fibroblasts, thence into opaque myofibroblasts, whose generation and deposition of abnormal extracellular matrix critically impacts the resulting loss of corneal transparency.[2] Transforming growth factor (TGF)-β1 is the major profibrotic cytokine active in this system, orchestrating physiological healing that includes fibrosis, but which can also lead to scar tissue.[3,4]

In the context of corneal wounding, TGF-β1 is a central mediator guiding stromal responses in fibroblast-to-myofibroblast conversion.[2] Fibrogenesis can be initiated through binding of TGF-β1 to its cognate receptor on the cell surface, resulting in phosphorylation of small mother against decapentaplegic (SMAD), its nuclear effector. Receptor-regulated SMADs (r-SMADs) can assemble into transcription regulatory complexes with partner SMADs (co-SMADs), translocating into the nucleus to directly regulate gene expression.[5–7] In addition to profibrotic gene regulation by SMADs, other intracellular signaling pathways can also contribute to fibrotic activation.[8] These non-SMAD signaling pathways may reinforce, attenuate, or otherwise modulate downstream cellular responses. For example, TGF-β1 can activate mitogen-activated protein kinases (MAPKs), phosphoinositide 3-OH kinases (PI3K), and several others, such as Rho-like GTPases and protein kinase A.[2,9] The non-SMAD- and SMAD-dependent pathways are often interconnected and display broad interactions to generate cell-type–specific or context-dependent TGF-β1 signaling.[10]

Over the past decade, evidence has emerged suggesting that mitochondria may play a role in TGF-β1–driven fibrosis. Mitochondria respire to generate ATP, but are also a major source of reactive oxygen species (ROS) that, although damaging when produced in excess, can also serve in a signaling capacity; as such, mitochondria are becoming recognized as a signaling hub for integrating cellular metabolic decisions.[11,12] Both pulmonary and cardiac mitochondria contribute to TGF-β1–driven fibrosis in the lung

and heart,[13,14] and metabolic reprogramming through mitocentric mechanisms contributes widely to fibrosis in many tissues (for recent reviews, see[15–17]). There are accumulating reports of ROS, redox, mitochondria, and metabolic reprogramming influencing TGF-β1's fibrogenic effects,[18–20] but how these processes functionally intersect with SMAD- and non-SMAD-dependent signaling to impact corneal fibrosis is entirely unknown.

Mitochondria exist as dynamically-regulated filamentous networks, which change shape and subcellular distribution by the balanced activity of two opposite processes—fusion and fission (fragmentation)—that function to meet cellular energetic and metabolic requirements.[21,22] Mitochondrial dynamics are predominantly mediated by large GTPases in the dynamin family, including dynamin-related protein 1 (DRP1).[23] This is of interest here because mitochondrial morphologic remodeling through DRP1-mediated fission has been shown to be necessary for TGF-β1-induced clinical phenotypes including kidney fibrosis,[24] cardiac fibroblast activation,[25] idiopathic pulmonary fibrosis,[26] and most recently, alkali burn–induced corneal injury.[27] Here we ask if this process is equally important for corneal fibrosis. Our goal was to define hitherto unknown physiological interactions between established molecular signaling cascades that integrate cellular metabolism with the process of TGF-β1–mediated differentiation of stromal fibroblasts into myofibroblasts. Our results lead to a complex interaction between noncanonical fibrotic mediators and mitochondrial fission that will serve as a foundation to better understand corneal wound healing.

Materials and Methods

Isolation, Culture, and Pharmacologic Treatment of Cat Corneal Fibroblasts. Primary feline corneal fibroblasts were generated as previously described[28] and in complete accordance with the ARVO Statement for the Use of Animals in Ophthalmic and Vision Research. In brief, fresh eyeballs were obtained immediately postmortem from adult, domestic short-hair cats (*Felis cattus;* Marshall Bioresources, North Rose, NY, USA). The corneal epithelium and endothelium were scraped off, and the stroma underwent double enzyme digestion with Dispase II (C756V28; Roche Diagnostics, Risxh-Rotkreuz, Switzerland) and Collagenase (*Clostridium histolyticum*; C8176; Sigma-Aldrich, St. Louis, MO, USA) overnight and 45 minutes, respectively.[28] Isolated stromal cells were grown in fibroblast growth factor–containing medium (no. C-23010; PromoCell GmbH, Heidelberg, Germany) at 37°C in a humidified chamber at 5% CO_2. After passage 2, the medium was changed to Dulbecco's modified Eagle medium (DMEM)–low glucose (no. D6406; Sigma Aldrich) with 15% serum (5% fetal bovine serum [FBS; no. F0926; Sigma Aldrich] + 10% newborn calf serum [no. 16010167; Gibco Laboratories, Gaithersburg, MD, USA]) and 1% (vol/vol) penicillin/streptomycin (no. 15323671; Corning Cellgro, New York, NY, USA) until they reached confluence. Harvested cells were cryopreserved at passage 3, and passage 6 to 9 post-thaw cells were used for all experiments.

In general, cat corneal fibroblasts were seeded into 35 mm wells at a density of 3×10^4 cells/cm^2. After the cells became adherent, the medium was changed to low glucose DMEM + 1% charcoal stripped FBS (DMEM-CSF; no. 12676-029; Gibco Laboratories), and the cells were incubated overnight to promote quiescence. Differentiation was induced using DMEM-CSF containing 1 ng/mL recombinant human TGF-β1 (R&D Systems Inc., Minneapolis, MN, USA). For data shown in the main figures of this article, pharmacologic inhibitors were added to separate wells 30 minutes before the addition of TGF-β1 and included (final concentration in DMEM-CSF) 10 µM of the DRP1 inhibitor *Mitochondrial division inhibitor-1 (*Mdivi-1; no. M0199; Sigma-Aldrich), 2.3 µM of the TGF-βR1 inhibitor SB431542 (no. S1067; Selleckchem, Houston, TX, USA), 10 µM of the ERK inhibitor U0126 (no. 662005; Calbiochem, San Diego, CA, USA), 10 µM of the JNK inhibitor SP600125 (no. S1460; Selleckchem), 5 µM of the p-38 inhibitor SB203580 (no. 559389; Calbiochem), or 2.5 µM of the PI3K inhibitor LY294002 (no. 440204; Calbiochem). Control groups had 0.1% dimethyl sulfoxide (Sigma Aldrich) substituted in place of inhibitors. Except for Mdivi-1, all of the inhibitors listed above have been used previously by our group on cat corneal fibroblasts maintained in similar culture conditions and in the context of TGF-β1-induced myofibroblast differentiation.[9,29] As such, the present experiments used previously ascertained optimal doses for each inhibitor. For Mdivi-1, we performed a preliminary dose-response experiment (Supplementary Fig. S1), which showed alpha-smooth muscle actin (α-SMA) expression to be reduced at doses ranging from 5–20 µM. This motivated our decision to run all remaining experiments in the present study with 10 µM Mdivi-1. It was also necessary to establish the time-course of DRP1 phosphorylation in our culture model; to this effect, we assayed control fibroblasts and cells exposed to 1 ng/ml TGF-β1 at 30 mins, 1 hr, 2 hrs, 4 hrs and 6 hrs (Supplementary Fig. S2). As the most significant differences between control and TGF-β1-treated cells were seen at 4 and 6 hrs of incubation, we decided to use the shorter time point (4 hrs) for the experiments outlined in Figure 4.

Fibroblast Imaging and Western Blot Analyses. Cell morphology was assessed using an Olympus IX73 microscope (Olympus America Inc., Center Valley, PA, USA). For western blotting, cells were washed and mixed with 2x SDS loading buffer (0.125M Tris-HCl, pH 6.8, 20% glycerol, 4% SDS, 0.004% bromophenol blue and added immediately before use with 0.1M DTT to generate whole-cell lysates as described.[30] The cell lysates were separated by molecular weight via electrophoresis on an 8% denaturing gel and transferred to nitrocellulose membranes. Ponceau S (#P7170; Sigma Aldrich) staining and β-Tubulin (1:5000; #sc-166729; Santa Cruz Inc., Dallas, Texas, USA) were used to verify that the same amount of protein was loaded in each lane.

Non-specific protein binding to the membrane was blocked using PBS containing 0.1% Triton-X100 (PBS-T) and 5% nonfat dry milk (#sc-2325; Santa Cruz Inc.). In order to maximize efficiency, membranes were often cut into pieces, each with a specific molecular weight range encompassing the target of interest; this allowed for multiple targets to be probed on a single blot without stripping and re-probing. Blots were incubated overnight at 4°C containing primary antibodies to the following targets at the dilutions indicated: Type 1 collagen (COL1; 1:2000; no. LF-68, kindly provided by Dr. Larry W. Fisher, NIH, Bethesda, MD, USA), total Fibronectin (t-FN; 1:2000; #H-300; Santa Cruz Inc.), α-SMA (1:10,000; no. MA5-11547; Thermo Fisher Scientific, Waltham, MA, USA), total SMAD 2/3 (1:2000; no. 8685; Cell Signaling Technology, Danvers, MA, USA), phosphorylated small mothers against decapentaplegic 3 (SMAD3) (S423+S425; 1:1000; no. P00059-1; Boster Technology, Pleasanton, CA, USA), phospho-p46/54

$JNK_{Thr183/Tyr185}$ (1:1000; no. 4671; Cell Signaling Technology), phospho-p38 $MAPK_{Thr180/Tyr182}$ (1:1000; no. 9215; Cell Signaling Technology), phospho-p44/42 $MAPK_{Thr202/Tyr204}$ (1:1000; no. 9106; Cell Signaling Technology), phospho-AKT_{Ser473} (1:1000; no. 4060; Cell Signaling Technology), total-p46/54 JNK (1:1000; no. 9252; Cell Signaling Technology), p-$Drp1_{Ser616}$ (1:500; no. 3455; Cell Signaling Technology), total-Drp1 (1:1000; no. 611112; BD Biosciences, San Jose, CA, USA), Opa1 (1:1000; no. 612606; BD Biosciences), Mfn1 (1:1000; ab57602; Abcam, Boston, MA, USA), Mfn2 (1:1000; no. M6319; Sigma Aldrich), and β-actin-HRP (1:5000; no. sc-47778; Santa Cruz Inc.). Commercial antibodies have been validated for target specificity by the manufacturers. The custom antibody for COL1 has been validated through extensive use and is currently distributed as an industry standard by Kerafast (Boston, MA, USA).

After several washes in PBS-T, secondary antibodies (anti-mouse IgG or anti-rabbit IgG-horseradish peroxidase; GE Healthcare, Chicago, IL, USA) were applied for one hour at room temperature. Bands were detected by Western Lightning plus-ECL (PerkinElmer, Waltham, MA, USA) or Super-Signal West Dura Luminol/Enhancer Solution (ThermoFisher Scientific). Finally, the membranes were scanned with a Chemi-doc machine (Bio-Rad, Hercules, CA, USA), and the resulting images were imported into Image J (NIH) for densitometric analysis, performed using standard protocols as previously described.[28]

Assessing Mitochondrial Morphology. Cat corneal fibroblasts with passage 6 were seeded at a density of 2.5×10^4 cells per cm^2 into glass-bottom plates (no. P12-1.5H-N; Cellvis, Sunnyvale, CA, USA) in low glucose DMEM containing 15% serum. After adherence, the media was switched to DMEM-CSF to induce quiescence, and the next day the cells were exposed to 1 ng/mL TGF-β1 in DMEM-CSF for times ranging from two hours to 48 hours. To visualize mitochondria, cells were incubated in DMEM-CSF containing 50 nM Mitotracker Red CMX-Rosamine vial (MTR; ThermoFisher Scientific) for 30 minutes, rinsed twice in DMEM-CSF, and imaged immediately via confocal microscopy as described below. In general, we aimed for three biological replicates, with 20 to 30 cells imaged per independent replicate. For inhibitor experiments, cells were preincubated in DMEM-CSF containing 10 µM SP600125, 10 µM U0126, or 2.5 µM LY294002 for 30 minutes before TGF-β1 treatment, and inhibitors were included in the media throughout the entire experimental time course.

Images of MTR-stained mitochondria were acquired using a Nikon A1R HD Laser scanning confocal microscope (Eclipse Ti2) equipped with a ×60 oil objective and running NIS-Elements version 5.11 software (Nikon Instruments, Melville, NY, USA). General acquisition parameters included using resonance scanner mode, 561 nm excitation, a 595/50 emission window, an image resolution of 1024 × 1024 pixels, PMT gain of HV = 10, and magnification ×2.78. Because of the thickness of fibroblasts, a z-stack with six steps and an optimal step size for the objective/pinhole was taken and converted to a maximum-intensity image. Images were saved as .nd2 files.

Custom code for image analysis was written in MATLAB (MitochondriaAnalysis.m) and ImageJ (MitochondrialMorphologyAnalysis.ijm). Our ImageJ Macro was heavily based upon existing code[31] (https://github.com/BoschCalvo2018/MitochondrialMorphologyAnalysis_Folder.ijm.git), modified to accommodate our specific images and MATLAB. Briefly, our code extracts mitochondrial morphology parameters from all images within a folder, allowing conserved metrics to be used in the analysis so as to minimize image-to-image variability, and relies on edge recognition to identify individual mitochondria. First, individual cells within an image were identified to create regions of interest. Second, segmentation algorithms in ImageJ were used to identify and analyze the mitochondrial network in each individual cell (region of interest). Two filtering parameters were used to accurately capture mitochondrial networks in each data set by reducing local background noise and smoothing the mitochondrial signal. Finally, two key parameters of mitochondrial morphology were computed: circularity ($\frac{4\pi * area}{perimeter^2}$) and form factor ($\frac{1}{circularity}$). Values for form factor close to 1 indicated a more rounded morphology, whereas higher values indicated a longer, more contiguous mitochondrial network within cells of interest. To assess fragmentation of the mitochondria, the average form factor was computed for each treatment group.

Statistical Analyses. To evaluate differences in protein expression levels on western blots, when three or more groups were compared, inter-group differences were tested with a one- or two-way analysis of variance (ANOVA), followed by either Tukey's or Dunnett's post-hoc tests, as appropriate. When only two groups were compared, a two-tailed Student's t-test was performed. A probability of error of $p < 0.05$ was considered statistically significant in all cases. To evaluate differences in mitochondrial morphology between three or more groups, Welch's one-way ANOVA was used with Dunnett's T3 post-hoc multiple comparison test or Tukey's HSD post hoc test. For two group comparisons, a two-tailed Student's t-test was performed.

Results

Mdivi-1 Decreases TGF-β1- Induced Expression of Profibrotic Molecules in Cat Corneal Fibroblasts

Basal expression of α-SMA in cat corneal fibroblasts cultured in 1% CSF was close to zero, while basal levels of COL1 and t-FN were low but distinctly above zero (lane 1, Figs. 1A, 1B). This is consistent with both prior observations,[9,30] as well as the notion that low levels of extracellular matrix components are generated by fibroblasts *in vitro*. After 2 days of culture with TGF-β1, α-SMA protein expression increased by ~32-fold, COL1 by nearly 4-fold, and t-FN by about 8-fold over baseline levels (Figs. 1A, 1B). Morphologically, cells changed appearance from the flat, elongated spindle shape of fibroblasts at baseline (Fig. 1C) to the more spread-out, balanced aspect ratio characteristic of myofibroblasts, with prominent stress fibers (Fig. 1D).

Mdivi-1 is a cell-permeable, selective inhibitor of mitochondrial fission.[32] Application of 10 µM Mdivi-1 alone did not alter baseline expression of the three proteins of interest (lane 4, Figs. 1A, 1B). However, pre-treatment with 10 µM Mdivi-1 dramatically diminished the impact of TGF-β1, with α-SMA expression increasing only eightfold relative to baseline, COL1 2.6-fold and t-FN 4.8-fold—significantly lower than values attained with TGF-β1 stimulation alone [two-way repeated-measures ANOVA: $F(2,17) = 1805$; $P = 0.0006$] but still higher than baseline [2-way repeated-measures ANOVA: $F(2,17) = 2995$; $P = 0.0003$]. Morphologically, these cells exhibited an intermediate phenotype between fibroblasts and myofibroblasts: although they were slightly larger and more multipolar than fibroblasts (contrast Figs. 1E and 1C),

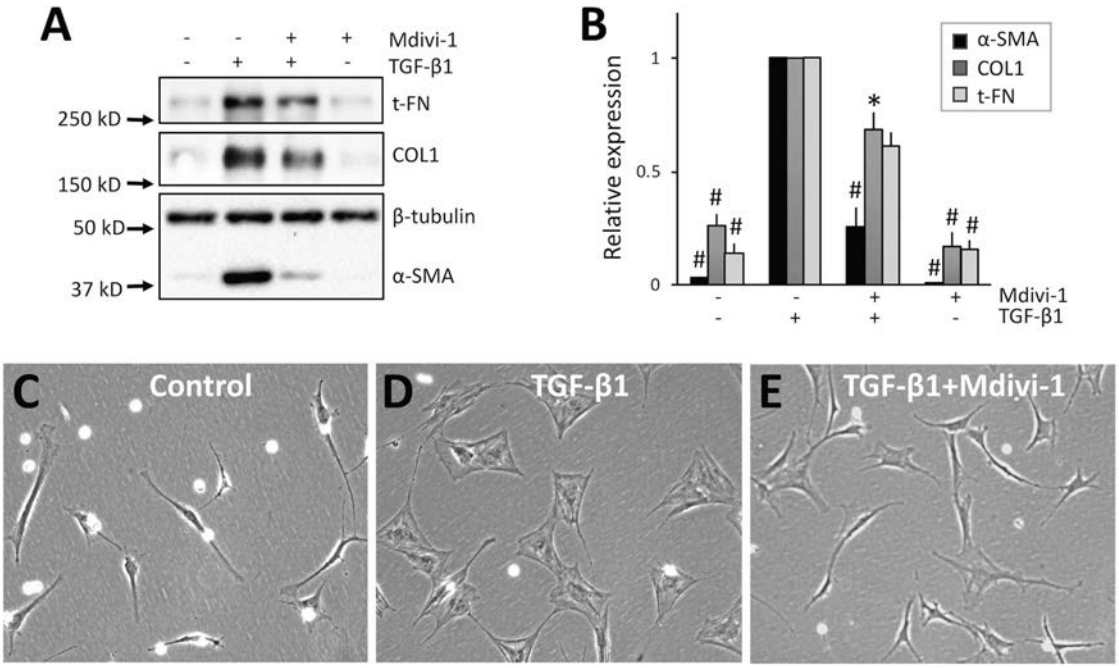

Figure 1. Mdivi-1 reduces TGF-β1-induced expression of α-SMA, COL1, and t-FN in cultured cat corneal fibroblasts. (**A**) Representative Western blots from cat primary corneal fibroblasts cultured for two days with 1 ng/mL TGF-β1 showing increased protein levels for α-SMA, COL1, and t-FN compared to control cells and suppression of this increase by 10 µM Mdivi-1. The β-tubulin levels were assayed as loading controls. (**B**) Plot of relative densitometry data for α-SMA, COL1, and t-FN expression relative to β-tubulin, normalized to values obtained in cells stimulated with 1 ng/mL TGF-β1 alone. Data shown are means ± SD over three experiments. One-way repeated measures ANOVAs demonstrated significant effects of treatments for all three molecules: α-SMA $F(3,11) = 267.8$, $P < 0.0001$; COL1 $F(3,11) = 41$, $P = 0.000216$; t-FN $F(3,11) = 22.74$, $P = 0.00112$. Significances from post-hoc Tukey's HSD tests relative to TGF-β1 are indicated on the graph: $^{*}P < 0.05$, $^{\#}P < 0.01$. (**C–E**) Representative phase contrast images of (**C**) unstimulated cat corneal fibroblasts, (**D**) fibroblasts exposed to TGF-β1 for two days, displaying typical, large, flattened, multipolar morphology of myofibroblasts, including prominent stress fibers, and (**E**) fibroblasts treated with both Mdivi-1 and TGF-β1. Note the persistence of many fibroblast-like cells, the scarcity of myofibroblasts, and the presence of intermediate cell morphologies (small, multipolar cells lacking stress fibers) in panel **E**.

they were not as large or rich in stress fibers as typical myofibroblasts (Fig. 1D).

TGF-β1 Stimulates Mitochondrial Fission in Cat Corneal Fibroblasts

The ability of Mdivi-1 to suppress the TGF-β1-induced fibroblast-to-myofibroblast transition suggested mitochondrial morphologic remodeling may be necessary for differentiation. Mitochondrial morphology can be assessed in live cells by fluorescent labeling with a targeted dye such as MTR (Figs. 2A, 2C). Skeletonization and segmentation of raw fluorescent images (Figs. 2B, 2D) is used to derive metrics for area, length, perimeter, circularity, and major/minor axis of each individual mitochondria in the cell; these metrics can then be applied to compute a shape representation termed form factor (FF). Higher FF denotes more elongated (i.e., less fragmented) mitochondria, whereas lower FF denoted more rounded (i.e., more fragmented) mitochondria. An initial time course of mitochondrial morphology after the addition of TGF-β1 to fibroblast cultures suggested that a statistically significant reduction in FF had occurred by 24 hours and that FF returned to baseline by 48 hours (Supplementary Fig. S3). These results were consistent with transient fragmentation of the mitochondrial network by TGF-β1, a finding that was further confirmed both qualitatively (Figs. 2A–D) and quantitatively (Fig. 2E). All in all, our data support the notion that TGF-β1 stimulates mitochondrial fission in early stages of fibrotic activation, with cells reaching a new homeostasis once in their new, differentiated state.

Impact of Mdivi-1 on Intracellular Signals Mediating the Effects of TGF-β1 in Corneal Fibroblasts

To more clearly outline the molecular nature of early events surrounding mitochondrial fission, phosphorylation of key profibrotic mediators of TGF-β1 signaling were examined using western analysis (Fig. 3). As previously reported,[9] incubation of cat corneal fibroblasts with TGF-β1 for 1 hour caused a large increase in levels of phosphorylated SMAD3 (compare lanes 1 and 2, Figs. 3A, 3B). Pre-incubation with the TGF-β1 receptor inhibitor SB431542 completely blocked this effect (lane 4, Figs. 3A, 3B), but preincubation with 10 µM Mdivi-1 did not (lane 3, Figs. 3A, 3B), suggesting that the ability of TGF-β1 to induce mitochondrial fission was unlikely to be SMAD3-dependent. Total SMAD2/3 levels were similar across conditions and did not change as a result of treatment with Mdivi-1 (Fig. 3A).

JNK, p38, ERK, and AKT can also be phosphorylated upon TGF-β1 activation.[9] Here, we show that Mdivi-1 completely blocked phosphorylation of both the p46 and p54 forms of JNK without affecting total JNK levels (Figs. 3C, 3D). In contrast, TGF-β1-mediated increases in phospho-

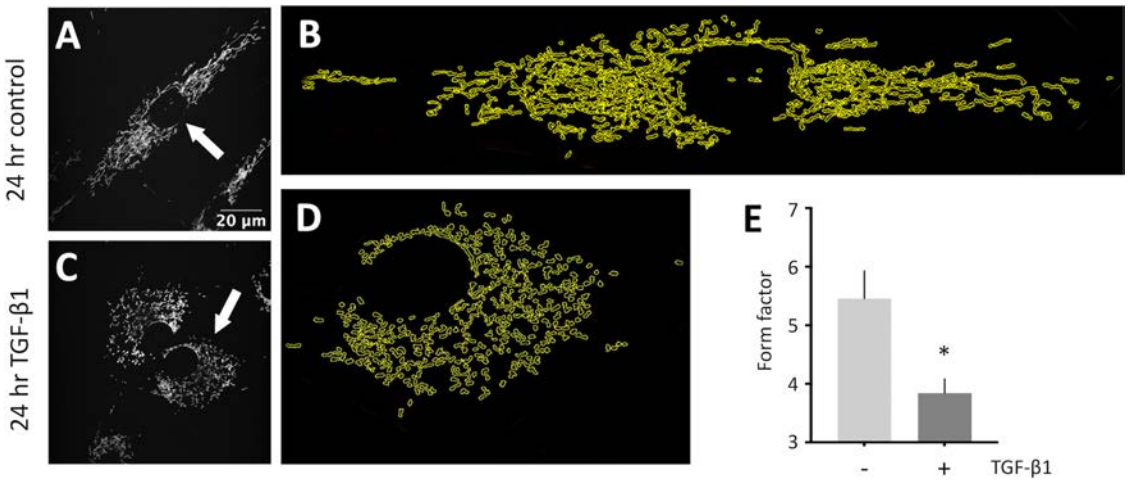

Figure 2. TGF-β1 stimulation causes mitochondrial fragmentation. (**A–D**) Live, cultured cat corneal fibroblasts labeled with MTR and imaged at 24 hours with/without 1 ng/mL TGF-β1. (**A, C**) Original fluorescence photomicrographs. (**B, D**) Processed (skeletonized), magnified versions of the *arrowed cells* in **A** and **C**, illustrating the automatically-segmented mitochondrial network (*yellow*), with fragmentation apparent in the TGF-β1 treated sample. (**E**) Plot of average form factor of three experimental replicates. *Error bars*: SEM. Number of cells analyzed for each replicate: control (32, 24, 13 cells), TGF-β1 (45, 25, 25 cells). Significance determined by unpaired *t*-test, with $^{*}P < 0.05$.

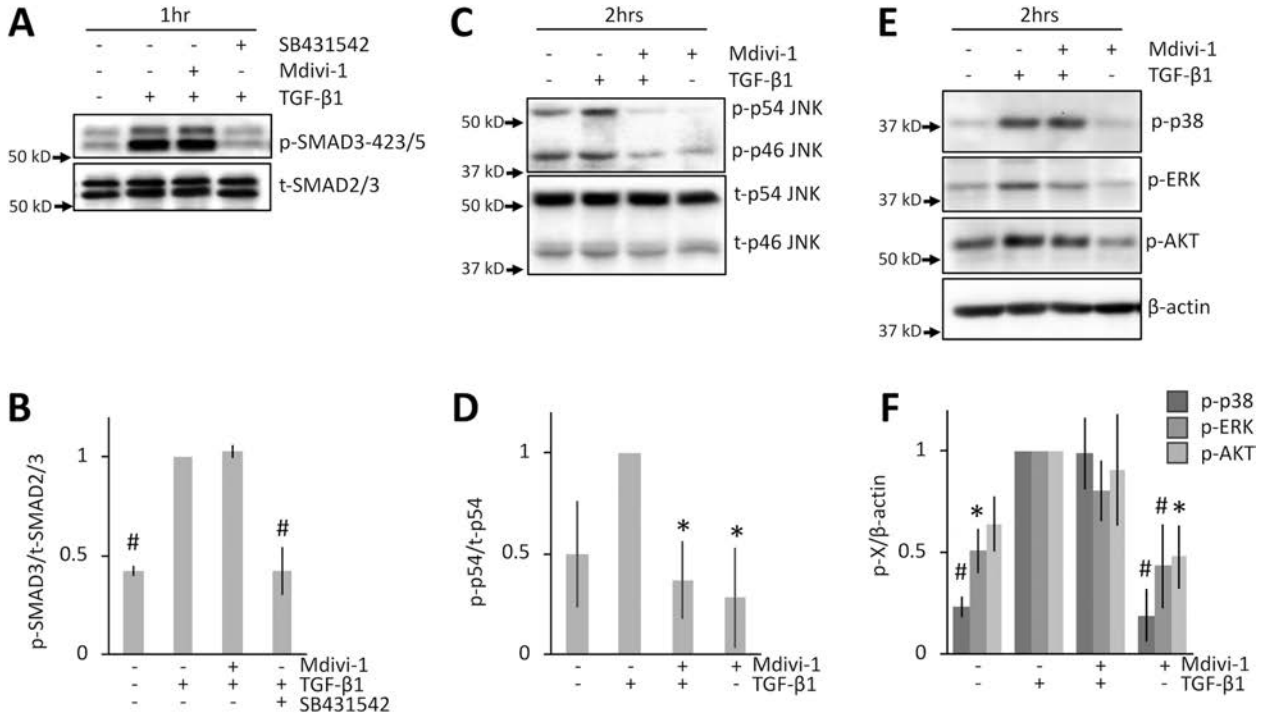

Figure 3. Intracellular mediators underlying anti-fibrotic effects of Mdivi-1. (**A**) Representative Western blot depicting phospho- and total-SMAD3 expression levels in protein extracts from cultured cat corneal fibroblasts. Cells were incubated $\pm$ 10 µM Mdivi-1, $\pm$ 1 ng/mL TGF-β1 and finally 2.3 µM SB431542 with 1 ng/mL TGF-β1, as indicated. (**B**) Plot of densitometric ratios for phospho-SMAD3 expression relative to total-SMAD2/3, normalized to the TGF-β1 treatment. One-way repeated measures ANOVA: $F(3,11) = 116.3$, $P < 0.0001$. Significances from post-hoc Tukey's HSD tests relative to TGF-β1 alone are denoted: $^{*}P < 0.05$, $^{\#}P < 0.01$. (**C**) Representative Western blots of corneal fibroblast extracts for phosphor-p54 and -p46 and total-JNK expression under the conditions indicated. (**D**) Plot of densitometric ratios for p-p54 JNK expression relative to total-p54 JNK, normalized to the TGF-β1 treatment. One-way repeated measures ANOVA: $F(3,11) = 7.48$, $P = 0.01884$. Significances relative to the TGF-β1 condition were computed and are denoted as in **B**. (**E**) Representative Western blot of corneal fibroblast extracts showing phospho-p38, phospho-ERK, and phospho-AKT expression levels under the conditions indicated. (**F**) Plot of densitometry ratios for phosphorylated proteins relative to β-actin, normalized to the TGF-β1 treatment. One-way repeated measures ANOVAs demonstrated significant effects of treatments for all 3 molecules: p38 $F(3,11) = 37.52$, $P = 0.0003$; pERK $F(3,11) = 11.12$, $P = 0.0073$; pAKT $F(3,11) = 8.85$, $P = 0.0127$. Significances from post-hoc Tukey's HSD tests relative to TGF-β1 are indicated as in **B** and **D**. For all graphs, data shown are means $\pm$ SD from 3 experimental replicates.

Investigative Ophthalmology & Visual Science

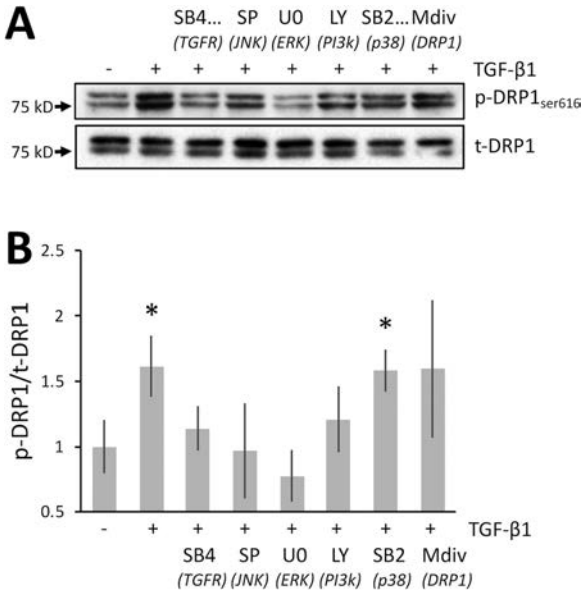

Figure 4. Effect of Mdivi-1, TGF-β1 and related intracellular signals on phosphorylation of DRP1$_{Ser616}$. (**A**) Representative Western blot illustrating phospho-DRP1$_{Ser616}$ and total-DRP1 expression in cat corneal fibroblasts treated with ± 1 ng/mL TGF-β1 for four hours, and pretreated with various inhibitors of noncanonical TGF-β1 signaling pathways: SB431542–TGF-β1 receptor (TGFR) inhibitor, SP600125-JNK inhibitor, U0126-ERK inhibitor, LY294002-PI3K inhibitor, SB203580-p38 inhibitor, Mdivi-1–DRP1 inhibitor. (**B**) Plot of densitometry ratios for phosphorylated DRP1$_{Ser616}$ relative to total-DRP1, normalized to the control condition (lane 1). Data are means ± SD from four experimental replicates. A repeated measures ANOVA (no sphericity assumed) showed a significant effect of treatment: $F(2.2, 6.6) = 6.18$, $P = 0.0295$. Significant, post-hoc, Dunnett's multiple comparison tests relative to baseline are denoted on the graph: $^{*}P < 0.05$.

p38, ERK1/2, and AKT levels were unaffected by preincubation with Mdivi-1 (Figs. 3E, 3F). Thus, of the many profibrotic, signaling molecules activated by TGF-β1 in corneal fibroblasts, JNK appeared to be the only one reliably impacted by Mdivi-1.

Interplay Between TGF-β1, Intracellular Profibrotic Signals, and DRP1$_{Ser616}$ Phosphorylation

DRP1 is the canonical mediator of mitochondrial fission, the mitochondrial target of Mdivi-1, and is regulated by mechanisms including selective phosphorylation, recruitment from the cytosol to the mitochondrial outer membrane, and protein oligomerization.[33,34] Here, we examined the impact of TGF-β1 signaling on selective phosphorylation of DRP1 at Ser$_{616}$, which is known to stimulate mitochondrial fission.[35] Consistent with the TGF-β1-mediated change in mitochondrial morphology (Fig. 2), a 1.6-fold increase in the ratio of p-DRP1$_{Ser616}$/t-DRP1 was observed four hours after TGF-β1 treatment (Fig. 4 and Supplementary Fig. S2).

Mitochondrial morphology reflects a balance between fission and fusion, with inner mitochondrial membrane protein Opa1 regulating inner mitochondrial membrane fusion and outer mitochondrial membrane proteins Mfn1 and Mfn2 contributing to outer mitochondrial membrane fusion. Reduced expression of pro-fusion proteins could result in apparent fragmentation, mimicking activation of DRP1. However, Western analyses suggested that there was no difference in the expression levels of these pro-fusion proteins between fibroblasts and myofibroblasts in culture (Supplementary Fig. S4). This result does not preclude a role for their acute regulation in the transient mitochondrial fragmentation observed during the process of fibroblast-to-myofibroblast transition, but it did motivate focusing further effort on deciphering the interaction of DRP1 phosphorylation with other pro-fibrotic signaling mediators.

To ascertain whether DRP1$_{Ser616}$ phosphorylation is influenced by activity of noncanonical signaling molecules activated by TGF-β1 in corneal fibroblasts, we examined the impact of specific inhibitors of JNK, ERK, AKT and p38 phosphorylation. In addition to regulating the TGF-β1-mediated fibroblast-to-myofibroblast transition through the noncanonical axis, several of these kinases are known to phosphorylate DRP1 directly (see Discussion for details). Our data showed that the upregulation of DRP1$_{Ser616}$ phosphorylation following TGF-β1 stimulation was suppressed at least in part by pre-incubation with inhibitors of JNK, ERK, and AKT, but not of p38 (Fig. 4). Finally, there are several competing mechanisms through which Mdivi-1 has been reported to inhibit fission, including by suppressing DRP1 phosphorylation, but our data with Mdivi-1 was ambiguous in this regard - DRP1$_{Ser616}$ phosphorylation status was not significantly different from either baseline or TGF-β1 stimulated (Fig. 4) at the 4 hours time point.

Finally, we tested whether inhibitors of the noncanonical TGF-β1 signaling axis could individually suppress de facto mitochondrial fragmentation, akin to their ability to suppress phosphorylation of DRP1$_{Ser616}$. Surprisingly, mitochondrial FF in cells treated with TGF-β1 together with either JNK, ERK, or AKT inhibitors was indistinguishable from cells treated with TGF-β1 alone (Supplementary Fig. S5). This suggests that none of these targets are independently required for TGF-β1-induced fragmentation. As such, we favor an interpretation where fragmentation is necessary and permissive for other pro-fibrotic signaling pathways, which act redundantly to assure morphologic remodeling. The implications of these results are discussed in greater depth below.

Discussion

In the present study, we used a primary cat corneal cell culture model of TGF-β1-induced fibroblast activation to probe—for the first time—the relevance of mitochondrial fission to corneal fibrosis. Our results show that TGF-β1 causes acute phosphorylation of DRP1 and mitochondrial fragmentation in corneal fibroblasts. We then demonstrate — also for the first time — that treatment with the mitochondrial fission inhibitor Mdivi-1 impedes TGF-β1-mediated corneal fibroblasts' transformation into myofibroblasts, both in terms of alterations to cell morphology and increased expression of molecular surrogates of the differentiated phenotype. To more critically address the relationship between mitochondrial fission and the regulation of fibrogenesis, both SMAD- and non-SMAD-dependent intracellular signaling pathway activation by TGF-β1 were assayed after Mdivi-1 treatment. Finally, pharmacological targeting of some of these pathways was used to ask whether they in turn contributed to the TGF-β1-dependent phosphorylation of DRP1 and de facto mitochondrial fission.

Investigative Ophthalmology & Visual Science

TGF-β1 signaling involves both canonical and noncanonical mechanisms, with the former tied closely to regulation of the SMAD transcription factors.[2,6,9,10] The observations made here that phosphorylation of SMAD3 by TGF-β1 signaling occurs independent of mitochondrial fission and on a time scale (~1 hour) where fragmentation of the mitochondrial network is only just becoming apparent suggest that the role of mitochondrial fission on TGF-β1-induced myofibroblast differentiation may be mediated through noncanonical signaling mechanisms. However, the exact nature of this role is complex. Our lab and others have defined the contribution of multiple signaling kinases that contribute to noncanonical TGF-β1-mediated effects in corneal fibroblasts.[9,29,36,37] Hence, we incorporated mitochondrial fission into these known pathways.

Clearly, inhibition of JNK blocked phosphorylation of DRP1, an important step in its activation (Fig. 4). JNK/DRP1/fission have been linked previously in the context of tumor suppression by the Hippo/Yap pathway,[38] acetaminophen toxicity through Receptor Interacting Protein Kinase-1,[39] and cardiac ischemia-reperfusion injury.[40] However, conversely and perhaps somewhat counter-intuitively, inhibiting mitochondrial fission through Mdivi-1 also blocked phosphorylation of JNK by TGF-β1 signaling (Fig. 3C). We interpret this to mean that fission is a positive regulator of JNK activation, suggesting a mechanism whereby these downstream effectors of noncanonical TGF-β1 signaling exhibit regulatory reciprocity, and perhaps form a communication axis that reinforces differentiation decisions.

Mdivi-1 is known to impair yeast Dynamin 1 (Dnm1) GTPase activity, likely via an allosteric binding mechanism that prohibits Dnm1 self-assembly,[32] and there are reports of DRP1 phosphorylation being suppressed by Mdivi-1.[41] However, Mdivi-1 has also been reported to be a selective inhibitor of mitochondrial Complex I (Cx-I).[42] This later off-target effect could influence the production of ROS through both forward and reverse electron transport mechanisms. As such, the involvement of Cx-I and/or Cx-I-derived ROS in JNK phosphorylation independent of mitochondrial fission remains a formal possibility.

Regarding the remaining signaling molecules tested here, ERK and AKT are clearly upstream regulators of DRP1 (Fig. 4) but are not themselves regulated by fission (Fig. 3), resulting in more linear signal transduction pathways (Fig. 5). ERK2 can mediate phosphorylation of DRP1 to drive tumor growth,[43] and the ERK-CREB pathway has been linked to BCL2/adenovirus E1B 19kDa-interacting protein 3 (Bnip3)-mediated mitophagy,[44] as well as to Activation-Induced Cell Death, a form of immune cell apoptosis where ERK regulates DRP1 together with JNK.[45] Similarly, the PI3K/Akt signaling axis has also been linked to DRP1 activation, for example, in the context of Alzheimer's Disease-relevant Amyloid beta (Aβ) signaling.[46] Moreover, both ERK and AKT have been shown recently to promote proliferation and invasion of lung adenocarcinoma through phosphorylation of $DRP1_{Ser616}$.[47]

However, it is essential to note that even requisite kinases do not necessarily phosphorylate DRP1 directly (i.e., why would inhibition of three separate kinases all block phosphorylation individually if such was the case?), and their effect may be cell-type specific. For example, under select circumstances, AKT can also *negatively* regulate DRP1 to prevent mitochondrial fission and promote cell survival.[48,49] Hence, our results do not preclude the involvement of intermediate kinases or alternative molecular signaling cascades that further inform these decisions. This point is emphasized by data showing that inhibition of JNK, ERK, or AKT, all of which block phosphorylation of DRP1 and inhibit the fibroblast-to-myofibroblast transition, do not individually prevent fragmentation of the mitochondrial network. It is worth noting that ERK inhibition had a subtle intermediate effect on is own and that the AKT + TGF-β1 data set was not statistically-significantly different from either the baseline or TGF-β1-treated data sets (Supplementary Fig. S5). However, neither of these observations alters the conclusion above.

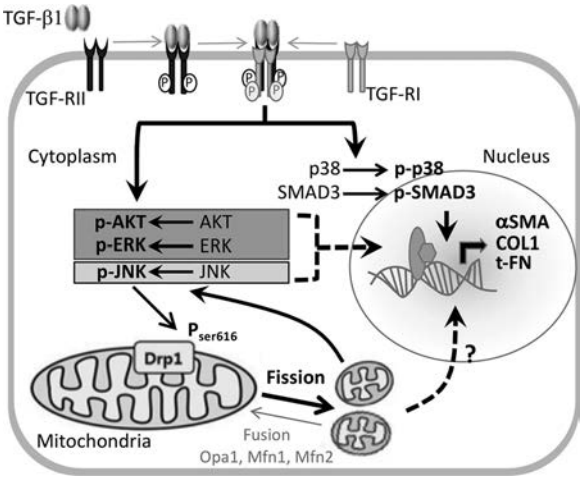

Figure 5. Putative role of mitochondrial fission in early stages of corneal myofibroblast differentiation. TGF-β1 dimerization and ligand binding to its cognate receptor TGF-RII recruits TGF-RI into a heteromeric complex, initiating a signal transduction cascade that can act through canonical and noncanonical pathways. The canonical TGF-β1 signaling pathway requires SMADs, which are directly phosphorylated by TGF-R1, transit to the nucleus, and regulate gene transcription (including a pro-fibrotic repertoire of targets such as a α-SMA, COL1, and t-FN). In contrast, noncanonical, non-SMAD pathways are activated directly by ligand-occupied receptors to modulate downstream effectors, such as p38, AKT, ERK and JNK kinases. Our results suggest that non-canonical AKT, ERK and JNK signaling pathways can modify DRP1, the central mediator of mitochondrial fission, and that TGF-β1 signaling causes a necessary fragmentation of the mitochondrial network early in the fibroblast-to-myofibroblast transition. Moreover, mitochondrial fission appears to reinforce JNK activation. In contrast, p38—although part of the noncanonical TGF-β1 signaling axis—does not appear to influence mitochondrial fission. However, it is important to note that first, our results do not preclude fission-independent roles for AKT, ERK, and JNK in fibrotic decision-making, and second, that neither AKT, ERK, or JNK is absolutely required for TGF-β1–mediated fragmentation, suggesting functional redundancy.

Moreover, although the Mdivi-1 result suggests that fragmentation is necessary for differentiation, these later results suggest that it is not sufficient to convey the effects of TGF-β1 in lieu of other presumed, non-mitochondrial functions of JNK, ERK, and AKT. Ultimately, the role of mitochondrial fragmentation, intertwined as it is in the noncanonical TGF-β1 signaling axis, may be to provide a metabolic context through which cell fate decisions are made—because mitochondrial fragmentation has also been closely tied to apoptosis and cell death.

In conclusion, our work demonstrates that mitochondrial fission integrates with fibrosis-relevant signaling pathways to support TGF-β1-mediated differentiation of corneal fibroblasts into myofibroblasts. This unexpected role may

herald a larger contribution of mitochondria acting to provide a metabolic context for competing cell fate decisions, such as whether TGF-β1 leads to differentiation or apoptosis.

Acknowledgments

The authors thank Margaret DeMagistris for technical assistance and regulatory support in obtaining and processing feline ocular tissues. The authors also thank Dr. George Porter (Department of Pediatrics, Cardiology) for critical reagents during extended revision of this manuscript.

Supported by the National Eye Institute (NEI) of the National Institutes of Health (R01 EY015836) and an unrestricted grant to the University of Rochester's Department of Ophthalmology from the Research to Prevent Blindness Foundation. K.W. was partially supported by an NEI Core Grant P30 EY001319 to the Center for Visual Science. A.K. was supported by NSF IOS1753742 and by a DeKiewet Fellowship from the University of Rochester.

Disclosure: **K.-I. Jeon,** None; **A. Kumar,** None; **K.T. Wozniak,** None; **K. Nehrke,** None; **K.R. Huxlin,** None

References

1. Wilson SE. Corneal wound healing. *Exp Eye Res*. 2020;197:108089.
2. Kamil S, Mohan RR. Corneal stromal wound healing: major regulators and therapeutic targets. *Ocul Surf*. 2021;19:290–306.
3. Frangogiannis N. Transforming growth factor-beta in tissue fibrosis. *J Exp Med*. 2020;217:e20190103.
4. Tzavlaki K, Moustakas A. TGF-beta signaling. *Biomolecules*. 2020;10:487.
5. Das P, Maduzia LL, Wang H, et al. The Drosophila gene Medea demonstrates the requirement for different classes of Smads in dpp signaling. *Development*. 1998;125:1519–1528.
6. Hata A, Chen YG. TGF-beta signaling from receptors to Smads. *Cold Spring Harb Perspect Biol*. 2016;8(9):a022061.
7. Hudson JB, Podos SD, Keith K, Simpson SL, Ferguson EL. The Drosophila Medea gene is required downstream of dpp and encodes a functional homolog of human Smad4. *Development*. 1998;125:1407–1420.
8. Zhang YE. Non-Smad signaling pathways of the TGF-beta family. *Cold Spring Harb Perspect Biol*. 2017;9(2):a022129.
9. Jeon KI, Kulkarni A, Woeller CF, et al. Inhibitory effects of PPARgamma ligands on TGF-beta1-induced corneal myofibroblast transformation. *Am J Pathol*. 2014;184:1429–1445.
10. Derynck R, Budi EH. Specificity, versatility, and control of TGF-beta family signaling. *Sci Signal*. 2019;12(570):eaav5183.
11. Spinelli JB, Haigis MC. The multifaceted contributions of mitochondria to cellular metabolism. *Nat Cell Biol*. 2018;20:745–754.
12. Shadel GS, Horvath TL. Mitochondrial ROS signaling in organismal homeostasis. *Cell*. 2015;163:560–569.
13. Gibb AA, Lazaropoulos MP, Elrod JW. Myofibroblasts and fibrosis: mitochondrial and metabolic control of cellular differentiation. *Circ Res*. 2020;127:427–447.
14. Veith C, Boots AW, Idris M, van Schooten FJ, van der Vliet A. Redox imbalance in idiopathic pulmonary fibrosis: a role for oxidant cross-talk between NADPH oxidase enzymes and mitochondria. *Antioxid Redox Signal*. 2019;31:1092–1115.
15. Mora AL, Bueno M, Rojas M. Mitochondria in the spotlight of aging and idiopathic pulmonary fibrosis. *J Clin Invest*. 2017;127:405–414.
16. Hamanaka RB, Mutlu GM. Metabolic requirements of pulmonary fibrosis: role of fibroblast metabolism. *FEBS J*. 2021;288(22):6331–6352.
17. Li X, Zhang W, Cao Q, et al. Mitochondrial dysfunction in fibrotic diseases. *Cell Death Discov*. 2020;6:80.
18. O'Leary EM, Tian Y, Nigdelioglu R, et al. TGF-beta promotes metabolic reprogramming in lung fibroblasts via mTORC1-dependent ATF4 activation. *Am J Respir Cell Mol Biol*. 2020;63:601–612.
19. Veith C, Hristova M, Danyal K, et al. Profibrotic epithelial TGF-beta1 signaling involves NOX4-mitochondria cross talk and redox-mediated activation of the tyrosine kinase FYN. *Am J Physiol Lung Cell Mol Physiol*. 2021;320:L356–L367.
20. Liu RM, Desai LP. Reciprocal regulation of TGF-beta and reactive oxygen species: a perverse cycle for fibrosis. *Redox Biol*. 2015;6:565–577.
21. Karbowski M, Youle RJ. Dynamics of mitochondrial morphology in healthy cells and during apoptosis. *Cell Death Differ*. 2003;10:870–880.
22. Kraus F, Roy K, Pucadyil TJ, Ryan MT. Function and regulation of the divisome for mitochondrial fission. *Nature*. 2021;590:57–66.
23. Hoppins S, Lackner L, Nunnari J. The machines that divide and fuse mitochondria. *Annu Rev Biochem*. 2007;76:751–780.
24. Wang Y, Lu M, Xiong L, et al. Drp1-mediated mitochondrial fission promotes renal fibroblast activation and fibrogenesis. *Cell Death Dis*. 2020;11:29.
25. Ding J, Zhang Z, Li S, et al. Mdivi-1 alleviates cardiac fibrosis post myocardial infarction at infarcted border zone, possibly via inhibition of Drp1-Activated mitochondrial fission and oxidative stress. *Arch Biochem Biophys*. 2022;718:109147.
26. Patel AS, Song JW, Chu SG, et al. Epithelial cell mitochondrial dysfunction and PINK1 are induced by transforming growth factor-beta1 in pulmonary fibrosis. *PLoS One*. 2015;10:e0121246.
27. Zhang K, Guo MY, Li QG, et al. Drp1-dependent mitochondrial fission mediates corneal injury induced by alkali burn. *Free Radic Biol Med*. 2021;176:149–161.
28. Huxlin KR, Hindman HB, Jeon KI, et al. Topical rosiglitazone is an effective anti-scarring agent in the cornea. *PLoS One*. 2013;8:e70785.
29. Jeon KI, Phipps RP, Sime PJ, Huxlin KR. Antifibrotic actions of peroxisome proliferator-activated receptor gamma ligands in corneal fibroblasts are mediated by beta-catenin-regulated pathways. *Am J Pathol*. 2017;187:1660–1669.
30. Jeon KI, Nehrke K, Huxlin KR. Semaphorin 3A potentiates the profibrotic effects of transforming growth factor-beta1 in the cornea. *Biochem Biophys Res Commun*. 2020;521:333–339.
31. Bosch A, Calvo M. Automated quantitative analysis of mitochondrial morphology. *Methods Mol Biol*. 2019;2040:99–115.
32. Cassidy-Stone A, Chipuk JE, Ingerman E, et al. Chemical inhibition of the mitochondrial division dynamin reveals its role in Bax/Bak-dependent mitochondrial outer membrane permeabilization. *Dev Cell*. 2008;14:193–204.
33. Chang CR, Blackstone C. Dynamic regulation of mitochondrial fission through modification of the dynamin-related protein Drp1. *Ann N Y Acad Sci*. 2010;1201:34–39.
34. Kraus F, Ryan MT. The constriction and scission machineries involved in mitochondrial fission. *J Cell Sci*. 2017;130:2953–2960.
35. Taguchi N, Ishihara N, Jofuku A, Oka T, Mihara K. Mitotic phosphorylation of dynamin-related GTPase Drp1 participates in mitochondrial fission. *J Biol Chem*. 2007;282:11521–11529.

36. Terai K, Call MK, Liu H, et al. Crosstalk between TGF-beta and MAPK signaling during corneal wound healing. *Invest Ophthalmol Vis Sci*. 2011;52:8208–8215.
37. Yang YH, Hsieh TL, Ji AT, et al. Stromal tissue rigidity promotes mesenchymal stem cell-mediated corneal wound healing through the transforming growth factor beta signaling pathway. *Stem Cells*. 2016;34:2525–2535.
38. Li H, He F, Zhao X, et al. YAP inhibits the apoptosis and migration of human rectal cancer cells via suppression of JNK-Drp1-mitochondrial fission-HtrA2/Omi pathways. *Cell Physiol Biochem*. 2017;44:2073–2089.
39. Dara L, Johnson H, Suda J, et al. Receptor interacting protein kinase 1 mediates murine acetaminophen toxicity independent of the necrosome and not through necroptosis. *Hepatology*. 2015;62:1847–1857.
40. Wang X, Song Q. Mst1 regulates post-infarction cardiac injury through the JNK-Drp1-mitochondrial fission pathway. *Cell Mol Biol Lett*. 2018;23:21.
41. Smith G, Gallo G. To mdivi-1 or not to mdivi-1: is that the question? *Dev Neurobiol*. 2017;77:1260–1268.
42. Bordt EA, Clerc P, Roelofs BA, et al. The putative Drp1 inhibitor mdivi-1 is a reversible mitochondrial complex I inhibitor that modulates reactive oxygen species. *Dev Cell*. 2017;40:583–594.e586.
43. Kashatus JA, Nascimento A, Myers LJ, et al. Erk2 phosphorylation of Drp1 promotes mitochondrial fission and MAPK-driven tumor growth. *Mol Cell*. 2015;57:537–551.
44. Li R, Xin T, Li D, Wang C, Zhu H, Zhou H. Therapeutic effect of Sirtuin 3 on ameliorating nonalcoholic fatty liver disease: the role of the ERK-CREB pathway and Bnip3-mediated mitophagy. *Redox Biol*. 2018;18:229–243.
45. Simula L, Corrado M, Accordi B, et al. JNK1 and ERK1/2 modulate lymphocyte homeostasis via BIM and DRP1 upon AICD induction. *Cell Death Differ*. 2020;27:2749–2767.
46. Kim DI, Lee KH, Gabr AA, et al. Abeta-induced Drp1 phosphorylation through Akt activation promotes excessive mitochondrial fission leading to neuronal apoptosis. *Biochim Biophys Acta*. 2016;1863:2820–2834.
47. Chung KP, Huang YL, Chen YJ, et al. Multi-kinase framework promotes proliferation and invasion of lung adenocarcinoma through activation of dynamin-related protein 1. *Mol Oncol*. 2021;15:560–578.
48. Ribeiro M, Rosenstock TR, Oliveira AM, Oliveira CR, Rego AC. Insulin and IGF-1 improve mitochondrial function in a PI-3K/Akt-dependent manner and reduce mitochondrial generation of reactive oxygen species in Huntington's disease knock-in striatal cells. *Free Radic Biol Med*. 2014;74:129–144.
49. Bhushan S, Malik F, Kumar A, et al. Activation of p53/p21/PUMA alliance and disruption of PI-3/Akt in multimodal targeting of apoptotic signaling cascades in cervical cancer cells by a pentacyclic triterpenediol from Boswellia serrata. *Mol Carcinog*. 2009;48:1093–1108.

Investigative Ophthalmology & Visual Science